Numerical investigation of turbulent-jet primary breakup using One-Dimensional Turbulence

Numerical investigation of turbulent-jet primary breakup using One-Dimensional Turbulence

A. Movaghar[1], M. Linne[2], M. Oevermann[1]

[1] *Department of Mechanics, Chalmers University of Technology, Gothenburg, Sweden*
[2] *School of Engineering, University of Edinburgh, Edinburgh, UK*

F. Meiselbach, H. Schmidt

Faculty of Mechanical, Electrical and Industrial Engineering, BTU Cottbus, Germany

Alan R. Kerstein

Consultant, 72 Lomitas Road, Danville, CA 94526, USA

Abstract

Primary breakup to form droplets at liquid surfaces is an important fundamental process to study as it determines the initial properties of the dispersed phase, which affect mixing rates, secondary breakup, droplet collisions, and flow separation within the dispersed flow region. Primary breakup can be regarded as one of the least developed model components for simulating and predicting liquid jet breakup. However, it is of paramount importance in many technical applications, e.g. fuel injection in engines and spray painting. This paper presents a numerical investigation of primary breakup of a turbulent liquid jet in still air at standard conditions using the one-dimensional turbulence (ODT) modeling framework. ODT is a stochastic model that simulates turbulent flow evolution along a notional 1D line of sight by applying instantaneous maps to represent the effect of individual turbulent eddies on property profiles. An important feature of ODT is the resolution of all relevant scales, both temporal and spatial. The restriction to one spatial dimension in ODT permits affordable high resolution of interfacial and single-phase property gradients, which is key

[1] Corresponding author, email: movaghar@chalmers.se

to capturing the local behavior of the breakup process and allows simulations at high Reynolds and Weber numbers that are currently not accessible to direct numerical simulations (DNS).

This paper summarizes our extensions of the ODT model to simulate geometrically simple jet breakup problems, including representations of Rayleigh wave breakup, turbulent breakup, and shear-driven breakup. Each jet breakup simulation consists of a short temporal channel section to initialize a turbulent velocity profile at the nozzle exit followed by an adjacent jet section. The simulations are carried out for jet exit Reynolds number of 11500, 23000, 46000 and 92000 while the Weber number is varied within the range 10^2 – 10^7. We present results on breakup statistics including spatial locations of droplet release, droplet sizes and liquid core length. The results on primary breakup are compared to experimental results and models.

Keywords: Spray, primary breakup, turbulence, one-dimensional turbulence

1. Introduction

The breakup of liquid jets is of paramount importance in many technical processes, e.g. injection of liquid fuel in engines, spray painting, and spray forming of metals. In the case of liquid fuel injection into engines, primary breakup determines initial droplet sizes and velocities and therefore impacts all subsequent processes such as secondary breakup, droplet collisions, droplet evaporation, and ultimately fuel-air mixing, which plays a central role in combustion efficiency and emissions.

The important influence of the atomization process on the overall system performance has led many researchers to focus on modeling and simulating liquid jet breakup and subsequent droplet formation with approaches ranging from fundamental investigations using DNS (Desjardins et al., 2008; Lebas et al., 2009; Shinjo and Umemura, 2011, 2010; Herrmann, 2011) and large-eddy simulation (LES) (Apte et al., 2003; Mahesh et al., 2006; Chesnel et al., 2011; Jhavar and Rutland, 2006; Dam and Rutland, 2015) to more applied engineering mod-

els based on the Reynolds averaged Navier Stokes (RANS) equations (O'Rourke and Amsden, 1987; Reitz, 1987; Tanner, 1997; Toninin et al., 2008).

In the latter engineering approach the gaseous phase is solved in an Eulerian frame whereas the dispersed phase is typically by modeled via Lagrangian parcels, each of which represents many droplets of a single size or a size distribution. The spray breakup process in these Eulerian-Lagrangian simulations can be modeled using standard deterministic breakup models based on Taylor analogy breakup (TAB) (O'Rourke and Amsden, 1987; Tanner, 1997) or wave models (Reitz, 1987). In both models, liquid blobs the size of the injector diameter are introduced into the simulation and undergo secondary breakup and atomization based on the balance between aerodynamic and surface tension forces acting on the liquid phase. Tuning is usually necessary every time the flow conditions are changed to achieve satisfactory results.

Apte et al. (2003) developed a stochastic secondary breakup model based on Kolmogorov's discrete model of breakup. The breakup process is simulated via a stochastic Fokker-Planck equation for the droplet radius. The model creates a broad spectrum of droplet sizes and the parameters of the model are computed dynamically based on the local Weber number, i.e. with less tuning than the standard blob model. However, the simulation starts by introducing computational blobs as in the models above. The model is applied in Apte et al. (2009) to simulate the atomization process in a gas-turbine swirl injector.

The above mentioned DNS and LES approaches are in principle capable of predicting primary breakup processes but due to computational costs they are usually limited to low Reynolds and Weber numbers. The number of grid points in a DNS needed to capture the physics increases with increasing Reynolds number, scaling as $Re^{9/4}$, which makes DNS (and LES in many cases as well) unfeasible for typical industrial applications with high Reynolds numbers and high Weber numbers.

There are only a few (simplified) models available for engineering applications which are actually simulating primary breakup. All have in common the use of an Eulerian description of the liquid phase close to the nozzle. The goal

is to describe realistically the dense zone of the spray and its atomization. In the ELSA (Eulerian-Lagrangian spray atomization) model (Vallet et al., 2001), additional Eulerian transport equations for the liquid mass and the liquid surface density are solved. Production and destruction of liquid surface density due to shear, turbulence, collisions, and evaporation are accounted for via modeled source terms (Lebas et al., 2005; Ning et al., 2007). Besides the Eulerian zone describing the dense region of the spray, the model features a transition zone to switch from the Eulerian to the Lagrangian calculation and a Lagrangian zone with classical tracking of droplets. The ELSA model is usually implemented in conjunction with RANS turbulence models. Although the model and its further developments and variants have been an important step forward in modeling the dense region of the spray it still needs tuning and the form of the interface density equation that is used remains open to discussion.

The lack of predictive primary breakup models is partly due to our incomplete knowledge of the underlying physics close to the nozzle. Only recently have experimental techniques like ballistic imaging (Linne, 2013; Linne et al., 2009) enabled detailed investigation of phenomena in the optically dense region of the liquid core of a jet. In addition, DNS (Herrmann, 2010; Lebas et al., 2009; Shinjo and Umemura, 2010) is now able to provide in-depth knowledge of primary breakup for moderate Reynolds and Weber numbers, which will help to develop and validate new models. Certainly, the development of a predictive model for primary breakup is highly desirable not only from an application point of view but also to gain a better understanding of the relevant physical processes.

The main objective of the present paper is the development of a new computational model for primary jet breakup that is both computationally efficient and more predictive than other low-cost approaches. We propose a new model for simulating and predicting primary jet breakup that is based on a stochastic one-dimensional approach, namely one-dimensional turbulence (ODT). We describe our extensions of the original ODT formulation (Kerstein, 1999; Ashurst and Kerstein, 2005) to gas-liquid multiphase flow to capture breakup mecha-

nisms such as Rayleigh breakup, turbulence induced breakup, and shear-driven breakup. The low computational costs of ODT compared to fully resolved three-dimensional DNS overcomes the limitation of DNS to moderate Reynolds and Weber numbers and therefore allows exploration of the full parameter range of technically relevant breakup regimes while maintaining high spatial and temporal resolution of relevant phenomena.

We apply our method to the simulation of the stationary breakup process of a planar jet in air at standard conditions and present results for the location of the onset of breakup at the jet surface, the liquid column length, and parameter dependences of droplet sizes. The main results are presented in the form of a breakup regime map as presented by Wu and Faeth (1995) and Sallam et al. (2002) and are compared to their experimental results.

The paper is organized as follows: After a description of the ODT model in the next section, we present a validation study of ODT for turbulence decay in a liquid jet without breakup based on comparison of the results to measurements. The validation is followed by the investigation and discussion of liquid jet breakup for a range of Weber numbers.

2. ODT formulation

2.1. Background and objectives

The ODT model of Kerstein used in this study is briefly described in this section. For a fully detailed description we refer to Kerstein (1999), Kerstein et al. (2001), and the variable-density extension by Ashurst and Kerstein (2005). ODT is a stochastic model of turbulent flows that solves the unsteady one-dimensional transport equations for mass, momentum, and optionally other scalars such as species mass fractions.

The main advantage of using one-dimensional unsteady stochastic simulation is that it enables affordable simulation of high-Reynolds-number turbulence over the full range of dynamically relevant length scales. In particular, it affordably resolves property gradients needed to capture details of jet primary breakup.

DNS provides such information for moderate Reynolds numbers but with much higher computational cost and a limited range of scales.

Meaningful applications of ODT are limited to relatively simple flow configurations, e.g. boundary layer flows (Kerstein, 1999), jets (Echekki et al., 2001) and mixing layers (Kerstein et al., 2001; Ashurst and Kerstein, 2005). For those flow problems ODT has been shown to produce the correct scaling laws and often to provide qualitatively and quantitatively good agreement with measurements and DNS results.

The present work focuses on modeling primary breakup along liquid turbulent jet surfaces and needs further extension of the ODT modeling approach. The successful application of ODT to multiphase flows may provide an additional tool for investigating such flows, especially if combined with DNS and experimental data.

2.2. Governing equations

The flows inestigated in this study are governed by the incompressible lorred Navier-Stokes equations for immiscible two-phase flow. The momentum equation is given by

$$\frac{\partial u}{\partial t} + u \cdot \nabla u = \frac{1}{\rho}\nabla p + \frac{1}{\rho}\nabla \cdot [\mu(\nabla u + \nabla^T u)] + \frac{1}{\rho} T_\sigma, \tag{1}$$

where u is the velocity, ρ the density, p the pressure, μ the dynamic viscosity and T_σ the surface tension force which is nonzero only at the phase interphase. All fluid properties are considered to be constant in each phase.

2.3. ODT configuration

In the ODT modeling approach we are not aiming at solving (1) directly, which is the target of direct numerical simulations (DNS), but instead look at a model analog for certain simple flow configurations. Here we are focusing on liquid jets into quiescent air. For such a flow configuration the ODT domain represents a lateral line of sight through the jet, which is assumed to be planar, and extends into the gaseous region on each side of the jet, see Fig. 1. The ODT

domain is treated as a Lagrangian object advected downstream with the liquid bulk velocity u_{bulk}. The fields defined on the 1D domain evolve then by two mechanisms: (1) molecular diffusion, and (2) a sequence of mapping operations, denoted eddy events, which represent the advection term in the Navier-Stokes equation along the ODT line. These eddy events occur over a large range of length scales, with frequencies that depend on instantaneous flow states. These mechanisms are described in detail in the following sections.

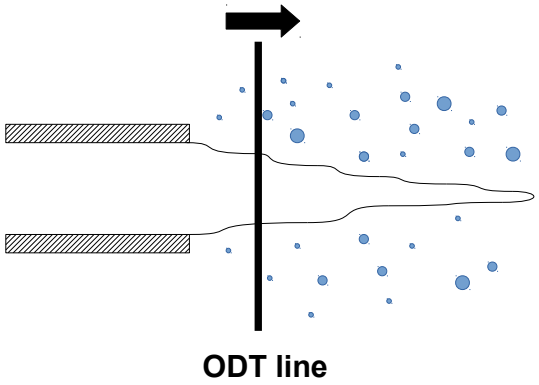

Figure 1: ODT line configuration for primary breakup simulations

The liquid initial condition, representing the flow state at the nozzle orifice, is generated by a channel flow simulation that is run to a fully developed statistically stationary state. During the subsequent jet simulation, liquid segments representing newly formed droplets are detached from the segment representing the residual liquid jet core. The detached segments are removed from the ODT domain, so at all times the multiphase representation consists of one liquid segment between two gaseous regions.

In the Lagrangian reference frame, a simulated ODT realization of the breaking jet represents advancement along the space-time trajectory $x = u_{bulk}t$. (Note the distinction between this and the flow state at a given instant, which is a function of the lateral coordinate y.) It is therefore not possible to capture x and t dependences individually, and in particular, transient jet development is not represented. Here, the model is applied solely to statistically stationary

jets, but it is possible that the model could represent transient jets usefully by empirically tuning model parameters to match measured transient states.

2.4. ODT time-advancement mechanisms

In contrast to common approaches based on the Navier-Stokes equations, ODT uses a set of time advancement mechanisms modeling different physical effects phenomenologically on a 1D line of sight through the turbulent flow.

The first mechanism is standard time evolution of flow properties by molecular diffusion, source terms, gravity, etc. described by a set of partial differential equations, but excluding advection. In this study of liquid jet breakup we assume constant densities ρ_l and ρ_g in the liquid and the gaseous phase, respectively. The only property transported across the phase interface is momentum. Therefore, the only flow properties that are time advanced by the first mechanism are the velocity components u_i governed by the truncated momentum equation

$$\frac{\partial u_i}{\partial t} - \nu_p \frac{\partial^2 u_i}{\partial y^2} = S_{p,i}, \tag{2}$$

where ν_p is the kinematic viscosity and the indices $i = 1, 2, 3$ denote streamwise, lateral and spanwise direction, respectively, with corresponding spatial coordinates (x, y, z). The subscript p is the phase label l for liquid and g for gaseous. In the present study, the 1D ODT line represents a lateral line of sight in the direction normal to a fixed wall (for channel flow) or to the gas-liquid interfaces of the planar liquid jet and its surrounding gas. For the channel flow simulation that initializes the flow state of the jet, the forcing term $S_{l,1}$ is assigned a fixed value

$$S_{l,1} = -\frac{1}{\rho_l}\frac{\partial p}{\partial x}$$

chosen such that the fully developed state matches corresponding experimental values of the jet exit Reynolds number and $S_{l,2}$ and $S_{l,3}$ are set to zero. Here $\partial p/\partial x$ is the mean pressure gradient that drives the channel flow. In the free jet part of the simulation no forcing is applied, i.e. the turbulence decays, except to the extent that possible shear in the gas phase contributes to liquid-phase turbulence through interfacial momentum coupling.

The second mechanism in ODT uses instantaneous maps to represent advection by 3D turbulent eddies. This eddy mechanism itself is divided into two mathematical operations representing turbulent advection and energy redistribution.

The first operation is a measure-preserving map, termed the triplet map, that represents stirring by a notional turbulent eddy. The second operation is a modification of the velocity profiles in order to implement momentum-conserving energy changes. Using the caret symbol to denote the post-eddy state, these operations can be written as

$$\hat{u}_i(y,t) = u_i(f(y),t) + b_i J(y) + c_i K(y) \tag{3}$$

and

$$\hat{\rho}(y,t) = \rho(f(y),t), \tag{4}$$

where as noted, ρ for given y and t has one of the two values ρ_l and ρ_g.

According to this formulation, fluid at location $f(y)$ is moved to location y by the mapping operation, thus defining the map in terms of its inverse $f(y)$. The terms $b_i J(y) + c_i K(y)$ affect only the velocity components and are used to capture pressure-induced energy redistribution among velocity components and other energy-conversion processes.

The triplet map compresses the original profile to one third of its original length l, pastes three identical compressed copies into the eddy range $[y_0, y_0 + l]$ and reverses the middle copy to avoid velocity discontinuities. The map can be summarized as

$$f(y) = y_0 + \begin{cases} 3(y - y_0), & \text{if } y_0 \le y \le y_0 + (l/3), \\ 2l - 3(y - y_0), & \text{if } y_0 + (l/3) \le y \le y_0 + (2l/3), \\ 3(y - y_0) - 2l, & \text{if } y_0 + (2l/3) \le y \le y_0 + l, \\ y - y_0, & \text{otherwise} \end{cases} \tag{5}$$

This mathematical formulation of the map satisfies measure preservation (conservation property) and continuity of mapped profiles.

In equation 3, $K(y)$ is a kernel function that is defined as $K(y) = y - f(y)$, i.e., corresponding to the distance the local fluid element is displaced. It is non-

zero only within the eddy interval. $J(y) = |K(y)|$ is an additional kernel whose coefficients b_i have a specified functional dependence on c_i and the density profile within the eddy that enforces momentum conservation. Hence the coefficients b_i do not introduce additional degrees of freedom and therefore the coefficients c_i are the unknowns to be determined through modeling.

The kinetic energy of an individual velocity component i is

$$E_i = \frac{1}{2} \int \rho(y) v_i^2(y) dy,$$

where the integration is restricted to the eddy interval, in which the eddy induces energy transfer and conversion. The amplitudes c_i in Eq. 3 are determined for each eddy individually by applying the following conditions:

1. The total kinetic energy $E \equiv \sum_i E_i$ is changed as needed to keep the total system energy constant, e.g. accounting for surface-tension potential-energy changes within the multiphase treatment.
2. The two additional needed conditions are obtained by requiring that the net available kinetic energy, defined as the total kinetic energy minus the lowest attainable kinetic energy based on unconstrained variation of the amplitudes c_i, is equally distributed among the three velocity components in order to simulate the tendency of turbulence to drive the flow toward isotropy, see Ashurst and Kerstein (2005) and Ashurst and Kerstein (2009) for details.

The jet is represented on the ODT domain as a single contiguous liquid region within some interval $[y_1, y_2]$. If the eddy range $[y_0, y_0 + l]$ is entirely within this interval or entirely outside this interval we have a single-phase eddy whose implementation is the same as in previous ODT formulations. If instead the eddy range contains one or both of the interfacial locations y_1 and y_2, we have a multiphase eddy requiring an extension of the ODT methodology; see below.

2.5. Eddy selection in ODT

ODT samples eddy events from an instantaneous distribution that evolves with the flow. These events are individually parameterized by position y_0 and size l.

The number of events during a time increment $\mathrm{d}t$ for eddies whose left boundary is located within the interval $[y_0, y_0 + \mathrm{d}y_0]$ on the ODT line in the size range $[l, l + \mathrm{d}l]$ is

$$\lambda(t; y_0, l)\, \mathrm{d}y_0\, \mathrm{d}l\, \mathrm{d}t,$$

where the event rate density λ can be expressed as

$$\lambda(t; y_0, l) = \frac{C}{l^2 \tau(y; y_0, l)}, \tag{6}$$

with dimension 1 / (length^2 time). The adjustable parameter C scales the overall eddy event frequency and τ denotes the eddy time scale. The eddy time scale $\tau(y; y_0, l)$ is evaluated using dimensional reasoning via

$$(l/\tau)^2 \sim E_{final} - Z(\nu^2/l^2), \tag{7}$$

where l denotes the eddy size and the first term on the right hand side is the final value of the available kinetic energy per unit mass, denoted E_{kin} in the absence of surface-tension effects, and the second term involving the parameter Z suppresses unphysically small eddies.

In practice it would be computationally unaffordable to reconstruct the distribution every time an eddy event or an advancement of Eq. 3 takes place. Therefore eddy events are sampled using an equivalent Monte-Carlo numerical procedure called thinning, see Ross (1996) for details.

2.6. Multiphase eddy implementation in ODT

As discussed above, if the eddy range contains one or both of the gas-liquid phase boundaries the eddy is treated as a multiphase eddy. Fig. 2.a shows an eddy which contains a phase change and hence is a multiphase eddy. Based on the main hypothesis of turbulent breakup theory, droplets can be formed by

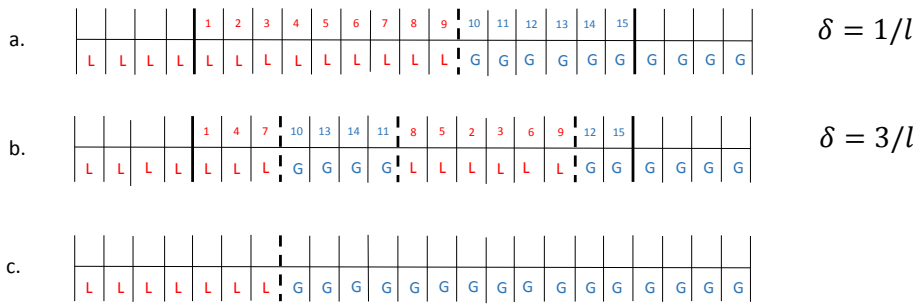

Figure 2: Multiphase eddy treatment in ODT. (a) The spatial region between the thick solid lines is selected for eddy implementation. It is a multiphase eddy containing both liquid (L) and gas (G) separated by one phase interface (thick dashed line). (b) A triplet map is implemented here as a permutation of the cells of a uniform spatial discretization of the 1D domain, illustrated by the reordering of cell indices within the eddy. Now there are three phase interfaces. (c) The newly formed droplet is removed and replaced by gas. Information about removed droplets can be transferred to a secondary-breakup sub-model within a comprehensive spray simulation.

turbulent eddies only when the kinetic energy of the eddy fluctuations is larger than the surface tension energy required to form a droplet of size corresponding the eddy that produces it. This needs modeling in ODT to account for the change of surface tension energy via an eddy. Incorporation of this into ODT starts from the volumetric energy density of surface tension $\sigma\alpha$, where σ is the surface tension energy per unit area and α is the surface area per unit volume. This gives an energy density

$$E_\sigma = \sigma\alpha/\bar{\rho} \tag{8}$$

per unit mass, where $\bar{\rho}$ is the mean density. The meaning and evaluation of α and $\bar{\rho}$ in ODT are considered.

Since an interface in ODT is represented by an isolated point on a line, geometric interpretation is required in order to obtain the area increase in the case of breakup. A plausible assumption for highly turbulent cases involving wrinkled interfaces is that the interface is a statistically homogeneous isotropic random surface. This does not necessarily apply to the jet breakup problems considered here, but it is convenient to adopt it as a universal assumption rather

than to attempt a case-by-case treatment. Based on geometric analysis (Chiu et al., 2013) showing that the number density n of interface intersections along a line of sight corresponds to an interface area per unit volume of $\alpha = 2n$, this assumption gives

$$E_\sigma = 2n\sigma/\bar{\rho}. \tag{9}$$

Because there are always exactly two phase interfaces on the ODT domain, the number of interfaces within any eddy is 0, 1, or 2, corresponding to number densities $n = 0$, $1/l$ or $2/l$, respectively, within the eddy. Triplet mapping of a phase interphase within an eddy produces three such interfaces. This is shown in Fig. 2.b. and can be interpreted as a tripling of interfacial area. In the Fig. 2.b. δ is defined as the increase of number density of interfaces due to triplet mapping which will be 0, $2/l$ or $4/l$ for the mentioned cases. Based on the stated assumption, the respective increases in interfacial area per unit volume are then 0, $3/l$, or $6/l$.

Multiplication of the area per unit volume increase δ by the surface tension σ gives the surface tension potential energy per unit volume that is stored in the newly created interfaces. This implies the surface tension energy change per unit mass

$$\Delta E_\sigma = 2\sigma\delta/\bar{\rho}, \tag{10}$$

where $\bar{\rho}$ is now identified as the mean density with the eddy range.

As noted earlier, conservation of total energy requires an equal and opposite change of the final kinetic energy. For a multiphase eddy, surface tension energy change is seen as a kinetic energy sink with the value $-\Delta E_\sigma$. Therefore the total energy formulation is re-written in the form

$$E_{final} = E_{kin} - \Delta E_\sigma. \tag{11}$$

As we focus on modeling primary breakup, droplets are removed from the computational domain as triplet maps create them by separating liquid from the jet, see Fig. 2.b. Fig. 2.c shows that the resulting gaps are set to gas-phase conditions, as explained later. Except for breakup events that contain the entire

liquid region (the model analog of liquid-column disintegration; see below), a triplet map can create only one droplet.

Droplets are removed because there is no suitable way to time advance their motion and interactions on the 1D Lagrangian domain. In any case, their subsequent fate is a question beyond the scope of the primary-breakup phenomenon addressed here. The ultimate goal of the present study is to develop a primary-breakup model in which the released droplets are inputs to a spray model of conventional form that then time advances droplet populations using probability distribution functions or other standard tools. With such coupling, the spray model could be used to characterize the droplet-laden gaseous medium in the ODT primary-breakup model, resulting in two-way coupling of the primary-breakup model and the spray model.

2.7. Jet disintegration mechanisms

The occurrence of an ODT eddy containing the entire jet is the model analog of jet disintegration, also termed liquid-core breakup. In the literature, three jet-disintegration mechanisms, each of which is dominant in a range of Weber numbers, with little dependence on Reynolds number, are usually reported (Wu and Faeth, 1993; Sallam et al., 2002; Wu and Faeth, 1995).

At low Weber numbers, the growth of Rayleigh waves on the liquid surface leads to eventual breakup. In the vicinity of Weber number 400, measurements suggest a transition to a different mechanism termed turbulent breakup. This regime has the same dependence of liquid-core length on x/D as the Rayleigh regime, but with a somewhat lower prefactor. The shift is subtle, and in earlier work the two regimes were subsumed in a single empirical correlation. Likewise, there is no attempt here to distinguish the two regimes. They are subsumed within a Rayleigh-breakup treatment that is described in section 2.8.

At Weber number of approximately 30,000, there is another transition to the third mechanism, termed bag/shear breakup, which is aerodynamically driven. The modeling of this mechanism is described in section 2.9 as part of a more general treatment of aerodynamic effects, though the approach is designed mainly

to capture aerodynamically driven jet disintegration.

2.8. Rayleigh term in ODT

A Rayleigh breakup term is incorporated into the ODT rate expression to model the effect of longitudinal surface waves that eventually cause disintegration of the jet, in contrast to the release of droplets due to the smaller-scale influences of turbulent fluctuations. The modified rate expression is

$$(l/\tau)^2 = E_{final} - Zv^2/l^2 + A(D/t_R)^2. \tag{12}$$

In the new Rayleigh energy term, A is an adjustable parameter, D is the local jet diameter and $t_R = \sqrt{\rho_l D^3/\sigma}$ is the Rayleigh time scale, defined as the time required for the Rayleigh jet instability to grow to size D, resulting in jet breakup (Wu and Faeth, 1993).

The Rayleigh term is included only for eddies that entirely contain one contiguous liquid region, which in the present application must be the jet region because droplets are removed from the simulation upon separation from the jet, as explained shortly. The Rayleigh term models the effect of longitudinal surface waves that eventually cause disintegration of the jet, in contrast to the release of droplets due to the smaller-scale influences of turbulent fluctuations.

2.9. Shear-driven breakup in ODT

At values of the jet exit Weber number exceeding 10^5, there is a transition to a different turbulent liquid column breakup mechanism (Sallam et al., 2002). At these conditions, turbulence distorts the liquid jet to a sufficient degree that an aerodynamic turbulent liquid column breakup mechanism becomes dominant.

As noted by Sallam et al. (2002) aerodynamic effects become important only when the liquid jet is in cross flow. For a jet with axial gas co-flow, this cross-flow configuration arises locally when the jet undergoes large scale distortions due to large scale instabilities. As these large distortions of the liquid jet are not captured by ODT, a model analog is needed to capture the effect on primary breakup.

The cross-flow effect is emulated by assuming a linear profile of the spanwise (z-directed) component gas phase velocity with linear time dependence $\pm S\,t$ of the slope, where t is the simulation time. This corresponds to a linear increase of shear with distance from the nozzle. The slope has opposite signs on opposite sides of the liquid core so that the formulation obeys statistical reflection symmetry with respect to the jet centerline. The shear coefficient S is tuned so that the simulation produces high Weber number liquid column breakup consistent with experimental observations; see section 3.2. The other two velocity components are spatially uniform in the gas phase. All gas velocity profiles are continually adjusted to match the corresponding liquid-phase velocity component at the liquid surface.

Time advancement governed by equation (2) includes momentum flux across the phase interface, so after each advancement step, the gas velocity profile deviates from linearity. Thereupon, the gas velocity profile is reset to the prescribed linear form on each side of the liquid core, shifted so that the gas and liquid velocities are equal at the liquid surface. The momentum transfer out of the liquid thus follows from equation (2), but the parameterization of the gas velocity profile supersedes the evolution of that profile resulting from the time advancement of equation (2). This reflects the physical picture that the gas flow is subject to external influences beyond the scope of the model that are subsumed in profile parameterization involving a tunable parameters. For present purposes, detailed physical modeling is needed only in the liquid phase.

Jet streamwise momentum change due to interfacial momentum transfer implies x dependence of the bulk velocity u_{bulk}. Indeed, droplet release also changes u_{bulk} because the droplet streamwise velocity (based on the average of u_1 over the droplet interval) is in general different from the jet bulk velocity. u_{bulk} in the relationship $x = u_{bulk}t$ is nevertheless held fixed at its value at the nozzle because these effects are small. Note that this relationship affects only the conversion from t to x for the purpose of gathering output statistics. Exact evaluation of $u_{bulk}(t)$ will be performed in the future if warranted.

The model representation of gas-phase shear promotes jet disintegration by

contributing to the available energy of eddy events containing the entire jet core. Unlike the modeling of the Rayleigh disintegration mechanism in section 2.8, which is applied only to that sub-class of multiphase eddies, the gas-phase representation is included in all multiphase eddies, meaning that it also contributes to the available energy of multiphase eddies that detach droplets from the jet core rather than encompassing the entire core. When such an eddy is implemented, the gas velocity profile is modified by triplet mapping, by the kernel operation, and by droplet removal, which implies introduction of gas into the void left by this removal. All these changes in the gas phase are superseded by immediate restoration of the prescribed linear shear, as is done also after each time-advancement step of the momentum equation.

Thus, the most fundamental difference between the Rayleigh-breakup treatment and the gas-phase treatment is that the former is used solely to model a mechanism of jet disintegration while the latter affects all time-advancement mechanisms and thus is a general-purpose though minimal treatment of the aerodynamic coupling. The aforementioned lack of information about external influences on the gas flow is subsumed in the parameter S that is tuned to reproduce the most important single effect of aerodynamical coupling on breakup, namely shear-induced jet disintegration.

Recalling from section 2.3 that the model represents a statistically stationary jet, the linear profile of gas velocity on either side of the jet can be viewed as a simple representation of the shear associated with jet-driven large scale secondary flow structures within the gas phase. To represent instead an early stage of unsteady injection, the time dependence of the imposed shear can be modified to reflect the high shear near the gas-liquid interface during the initial transient. As noted in section 2.3, modeling of transient regimes is not attempted here.

This physical interpretation implies shearing of the streamwise velocity profile, but in the model, the shear is applied to the spanwise profile. As noted, this is intended to represent the cross-flow shearing effect. Because ODT does not have a representation of local rotation of the interface orientation, the cross-flow configuration is represented by rotating the gas shearing so as to emulate a cross

flow relative to jet streamwise motion.

The gradual time development of secondary flow structures in the jet motivates the adopted cross-flow representation involving time-increasing shear. In addition to being simple and convenient, the assumed linear time dependence of the shear implies a dependence of the liquid column breakup length on ρ_l/ρ_g that has previously been derived theoretically and confirmed experimentally.

To estimate the density-ratio dependence implied by the model, consider an idealization of the flow state within some eddy that induces liquid column breakup. It has some size L that is of order D, where it is assumed that the size of the liquid core region is not much less than its initial value D when the breakup occurs. For estimation purposes, the eddy interval is assumed to consist of liquid and gas regions that are roughly equal in size, where, as assumed, the spanwise shear in the gas region is uniform with magnitude St at the breakup time t. The liquid region has velocity fluctuations that are much smaller in scale than L due to turbulent homogenization of the large-scale (order-D) lateral flow structure of the jet during the time interval t. Any interfacial layers induced by the gas-phase shear are likewise much smaller than L.

As indicated by Eq. 7, the eddy time scale τ is determined by a measure E_{final} of the kinetic energy content of the ODT velocity profiles within the eddy interval and by a viscous correction that mainly affects small eddies and therefore is neglected for estimation purposes. In Eq. 11, E_{final} is expressed as a kinetic energy term E_{kin} minus a quantity representing eddy-induced kinetic-energy conversion to surface-tension potential energy. The latter term is likewise neglected, corresponding to a high-Weber-number assumption, so the right-hand side of Eq. 7 reduces to E_{kin}.

E_{final} is a measure of the kinetic energy associated with velocity variations of order-L spatial extent within the eddy interval. Specifically, it is the net available kinetic energy determined using the kernel procedure outlined in item 2 of the enumeration in section 2.4. Indeed, this procedure is formulated specifically for the purpose of capturing only the contributions by velocity variations of order-L spatial extent because these are the flow features that provide the

shear forcing for size-L eddy turnover.

In Eq. 7, simplified as stated so that the right-hand side reduces to E_{kin}, energy is expressed per unit mass. The simplified equation is recast in terms of volume-integrated energy within the eddy interval. Here, the eddy volume is taken to be the ODT eddy size L times a nominal cross-sectional area that multiplies both sides of the equation and therefore is dropped. On this basis, the left-hand side scales as $\rho_l L^3/\tau^2$, where the average density within the eddy interval is taken to be of order ρ_l because $\rho_g \ll \rho_l$. On the right-hand side, the eddy-integrated available energy is denoted Q for consistency with Ashurst and Kerstein (2005). Q is analogous to Q_2'' in Eq. 1 of Ashurst and Kerstein (2009), where the subscript indicates that τ was evaluated based on the net available kinetic energy of component 2, but for reasons explained in section 3.4 of Kerstein and Wunsch (2006), the net available kinetic energy Q summed over velocity components has been used in subsequent work, including the present study.

Q is the sum of the component available energies Q_i that are defined by Eq. (26) of Ashurst and Kerstein (2005). Expanding that equation based on the definitions of the terms on the right-hand side (subject to the corrections in Ashurst and Kerstein (2009)), various integrals over ρ or ρv_i times powers of J and K are introduced. For the representative case under consideration, the integrals involving ρ scale as ρ_l because $\rho_l \gg \rho_g$. Those involving ρv_i scale as ρ_g because the small-scale fluctuations of v_i within the jet effectively nullify the contribution from the liquid region. (Nonzero spatially uniform contributions are similarly nullified due to a subtraction operation mentioned in item 2 of the enumeration in section 2.4.) The net outcome is that Q scales as $\frac{\rho_g^2}{\rho_l} L^3 (St)^2$.

The various estimates of quantities in the simplified form of Eq. 7 give, after rearrangement, $St\tau \propto \rho_l/\rho_g$. Jet column breakup is deemed to occur when the turnover time τ of the typical breaking eddy matches the elapsed time t. Therefore t is substituted for τ, giving $t \propto (S^{-1}\rho_l/\rho_g)^{1/2}$. Owing to the near constancy (here approximated as exact constancy) of the jet bulk velocity, x is proportional to the fluid residence time t, so the jet column breakup length is

ODT parameter	Value
C (eddy frequency)	12.5
Z (viscous term)	50
A (rayleigh term)	1.5
S (shear)	40 $1/s^2$
β (elapsed time criterion)	0.14

Table 1: Summary of ODT breakup model parameters

estimated to be proportional to $(\rho_l/\rho_g)^{1/2}$.

In section 3.2.2 it is noted that this square-root dependence of the breakup length on the density ratio has been observed experimentally and explained theoretically based on elementary considerations. This dependence is not an intrinsic property of ODT because it is contingent on the assumption that the aerodynamic shear resulting from the postulated cross-flow mechanism is linear in t and therefore in x. Though simple and plausible, this assumption has no first-principles justification. However, the fact that it yields a scaling property that is independently known to be valid can be viewed as an *a posteriori* fundamental justification, thus indicating that the assumed linearity is not entirely arbitrary. This does not establish that jet instabilities do in fact lead to a linear-in-time effective aerodynamic shear coupling because ODT does not fully capture the relevant underlying physics. It remains to be investigated whether the ODT jet-breakup behavior that follows from linear-in-time shear is anything more than purely fortuitous.The model parameters are summarized in Table 1.

3. Results

3.1. Liquid jet with no breakup

Before investigating jet breakup behavior, the evolution of turbulent intensity in the jet prior to breakup is examined. This ensures that ODT is capable of correctly predicting the level of turbulence prior to breakup within the jet. The investigations are similar to those presented in Schulz et al. (2013) with

some important changes of the ODT setup to improve the results. These new changes are based on a parameter study done by the authors to optimize ODT model parameters C and Z to improve the simulation results compared to experiments. As discussed in section 2.5, C and Z are the ODT global parameters which have been kept at the same value for liquid jet both with and without breakup. More details of this parameter calibration are reported in Meiselbach (2015).

Wolf et al. (1995) performed measurements of the mean velocity and turbulence intensity for a rectangular jet of water ejecting under isothermal conditions into ambient gas at streamwise locations up to 30 nozzle widths, which is where breakup starts at the jet surface. The primary nozzle is a parallel plate channel with a rectangular cross section of width 10.2 mm in the narrower direction. The liquid jet has low Weber number. This leads to no droplet generation at the surface of liquid jet until it breaks beacuse of the Rayleigh waves.

The ODT representation of this experiment consists of two parts: a short temporal channel section and the jet section. The simulation starts from a fully developed turbulent channel flow profile of water at standard conditions. The Dirichlet (no-slip) boundary condition is applied to the velocity components during the channel section. The channel flow is simulated for a time duration of $t = D/u_{bulk}$, where D denotes the channel width and u_{bulk} represents the bulk velocity. At this point the current flow properties are saved as new restart profiles for the next realization of the channel flow and are used as initial conditions for the jet portion of the simulation. The switch to jet simulation done by changing the boundary condition of the current realization from no-slip to a Neumann (free-slip) boundary condition. This precludes any momentum exchange with the surrounding gas across the phase boundary, reflecting the near absence of momentum transfer to the gas in the experimental configuration, so the liquid jet is effectively a self-contained entity and no representation of the gas phase is required.

For the channel flow portion of the simulation, the model parameters are adjusted to match the results of the DNS channel flow simulation by Moser

et al. (1999) and measurements by Hussain and Reynolds (1975), giving $C = 7$ and $Z = 400$. Previous ODT channel-flow simulations are reported by Schmidt et al. (2003) and Schulz et al. (2013). Here, as in those studies, the largest eddy size is $l = D/2$ in the channel portion.

For comparison of ODT results with the experiments by Wolf et al. (1995), the imposed mean pressure gradient in the channel part was chosen to match the experimental bulk Reynolds number. For the jet part, the simulations were carried out with model constants set to $C = 12.5$, $Z = 50$, and largest eddy size D, values that were chosen by Schulz et al. (2013) for a good fit to the Wolf et al. measurements.

Based on the available experimental data for two different Reynolds numbers, $Re_{bulk} = 23000$ and 46000, two main flow simulation results are of interest, namely mean velocity profiles and profiles of the turbulence intensity.

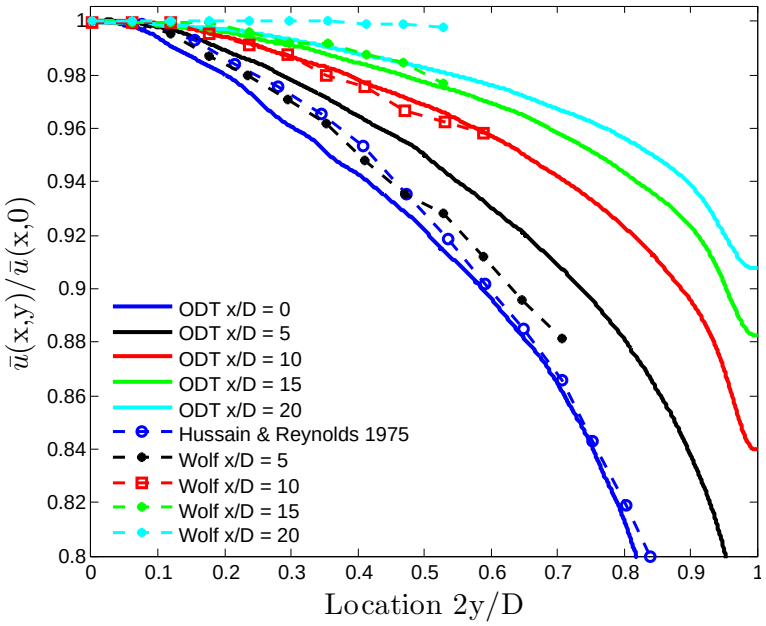

Figure 3: Mean streamwise velocity profiles (where $y = 0$ denotes the mid-plane) at several spatial positions for $Re_{bulk} = 23000$.

Fig. 3 presents the mean velocity profile at different axial locations for

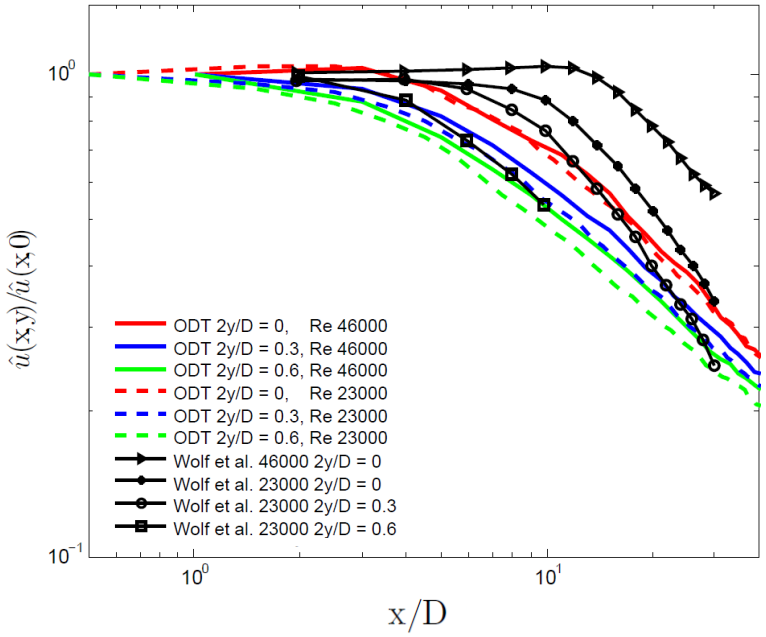

Figure 4: Comparisons of streamwise turbulence intensity $\hat{u}(x,y) = u_{rms}(x,y)/\bar{u}(x,y)$ with measurements by Wolf et al. at different lateral positions for different Reynolds numbers $Re_{bulk} = 23000$, $Re_{bulk} = 46000$.

$Re_{bulk} = 23000$. As it shows, the initial profile reflects quite well the result of Hussain and Reynolds (1975) for the fully developed channel flow. The profiles at positions $x/D = 10, 15$ have the best fit with the experiments. The curve at $x/D = 5$ has the same tendency but shows a noticeable deviation from the experiments done by Wolf et al. (1995). This can be explained by the fact that ODT is a 1D model and that it cannot capture 3D effects at the outlet of the channel caused by changes of the boundary conditions and the pressure field. Another such 3D effect is the so called *bending effect* discussed in Lignell et al. (2013). The ODT model domain is interpreted as a straight line advected at the bulk velocity without distortion. In reality, a straight Lagrangian line at the nozzle exit would be bent due to the lateral variation of the mean axial velocity. This effect, which is most prominent in the near field where the lingering influence of the channel flow is greatest, is ignored here with the consequence

that the outer regions of the ODT domain are advected too rapidly, so they have less time to undergo turbulence decay than expected after being advected a given streamwise distance from the nozzle exit.

The ODT results for $x/D = 20$ show a higher slope than the experiments. As discussed in Schulz et al. (2013) and Gonzalez-Juez et al. (2011), in confined flows with a free-slip surface, DNS predicts an increase of the tangential velocity fluctuations near the free-slip surface while ODT predicts a decrease since it can not capture the mechanism that causes this, which is development of quasi-2D flow near the free-slip surface. The jet simulated in this paper behaves similarly near free-slip surface, explaining why ODT cannot predict the experiments accurately in the far field.

Fig. 4 shows the spatial evolution of the turbulence intensity at lateral positions $2y/D = 0.0$, 0.3 and 0.6 for Reynolds numbers 23000 and 46000. Whereas the slopes, i.e. the decay rate of turbulence, are well captured by ODT, the onset of the decay for different lateral positions shows substantial deviations from the experiments of Wolf et al. The computed curve for $2y/D = 0.6$, however, shows reasonable agreement with the measurements. The capability of ODT to capture decaying turbulence close to an interface qualitatively and quantitatively correctly is important for the liquid jet breakup simulation below in order to correctly capture the contribution of liquid-phase turbulence to droplet release. Therefore, the empirical ODT parameters have been tuned to match turbulence decay close to the gas-liquid interface and not, as usual, at the centerline.

A comparison of the experimental results for two different Reynolds numbers shows that with increasing Reynolds numbers the turbulence decay rate is decreasing and the onset of decay is delayed. The corresponding simulation results show weaker Reynolds-number dependence.

3.2. Liquid jet with breakup

3.2.1. Numerical implementation

As noted earlier in section 3.1 the liquid jet simulation contains two part, a short temporal channel section followed bu temporal jet section. At liquid

jet with breakup simulation the change between sections is implemented by changing the boundary condition, from Dirichleth boundary condition during the channel simulation to free slip boundary condition during the jet simulation. The interfacial flux matching condition is conserved during jet simulation. The change between sections is implemented by changing the boundary condition and increasing the domain length to 3D, where D is the channel width. The domain length should be large enough so that the finite size of the domain does not affect the results. For the jet part, the simulation was carried out with model constants same as section 3.1, $C = 12.5$, $Z = 50$.

3.2.2. Streamwise development of the breaking jet

The validation in section 3.1 of ODT for the cases prior to breakup initiation was a foundation for application of ODT to breakup cases, in particular enabling the tuning of model parameters based on liquid-phase turbulence measurements that have not been performed during jet breakup. Generalizing the model to capture the physical mechanisms related to breakup introduced additional modeling parameters in the ODT formulation which need to be optimized. Some of these modeling parameters were discussed in section 2. Another is discussed next.

For the jet section the eddies inside the liquid core are always be smaller than the local jet diameter but multiphase eddies larger than the jet local diameter are allowed. The elapsed-time criterion described in Echekki et al. (2001) limits the allowed sizes of the multiphase eddies during the jet simulation. The criterion excludes multiphase eddies whose τ value violates the requirement $\tau > \beta t$, where t is the elapsed time since the start of the jet part and β is an adjustable parameter.

The physical justification of this restriction is that an ODT eddy event is interpreted as the completion of an eddy motion of finite time duration. Therefore the event should be allowed only if the elapsed time exceeds the turnover time of the corresponding physical eddy. The adjustable parameter is introduced because this is a scaling concept rather than an exact physical relationship.

Parameter	Value	
	Baseline	Variations
μ_l (Liquid absolute viscosity)	8.94×10^{-4} kg/ms	$[4.47 - 17.88] \times 10^{-4}$ kg/ms
μ_g (Gas absolute viscosity)	18.5×10^{-5} kg/ms	$9.25 \times 10^{-5} - 37 \times 10^{-5}$ kg/ms
D (Initial jet diameter)	10.2 mm	10.2 mm
u_{bulk} (Jet exit mean velocity)	2 m/s	$[1, 2, 4, 8]$ m/s
ρ_l/ρ_g (Liquid/gas density ratio)	860	$16 - 860$
$Re_{bulk} = \rho_l u_{bulk} D/\mu_l$ (Reynolds)	23000	$11500, 23000, 46000, 92000$
$We = \rho_l u_{bulk}^2 D/\sigma$ (Weber)	10^7	$10^2 - 10^7$
$Oh = \mu_l/(\rho_l D\sigma)^{0.5}$ (Ohnesorge)	0.0138	$0.0034 - 0.0138$

Table 2: Summary of simulation conditions for the liquid jet

Turbulent eddies entirely contained within the liquid phase turbulence already became fully developed during the channel flow simulation that precedes the jet simulation, so no waiting time is required for these eddies to complete their turnovers in the jet region. This criterion is the ODT analog of previous dimensional estimation of breakup onset locations based on the relevant eddy turnover time or other applicable time scales such as the Rayleigh time scale as described in Wu and Faeth (1993).

In ODT, liquid-column breakup corresponds to the occurrence of an eddy containing the whole liquid region. As discussed in the modeling section, for such eddies a Rayleigh term is included in the expression determining eddy likelihood. The parameter A in the ODT Rayleigh term has been adjusted to obtain quantitative agreement of two statistical measures of ODT column length with those lines, which roughly represent the experimental observations of liquid-column breakup at relatively low Weber number. Likewise, the shear parameter S has been adjusted to match experimental observations of liquid-column breakup in the high-Weber-number regime. The test conditions of the current study are summarized in Table 2.

Simulations were performed for the turbulent planar jet with jet exit liquid

565 Weber numbers in the range $We = 10^2 - 10^7$ and for bulk Reynolds numbers of $Re_{bulk} = 11500, 23000$ and 46000. The bulk Reynolds numbers are varied by varying u_{bulk}. The ranges of variation of the other variables in the current study are summarized in Table 2. Results are compared with Wu and Faeth (1995) and Sallam et al. (2002).

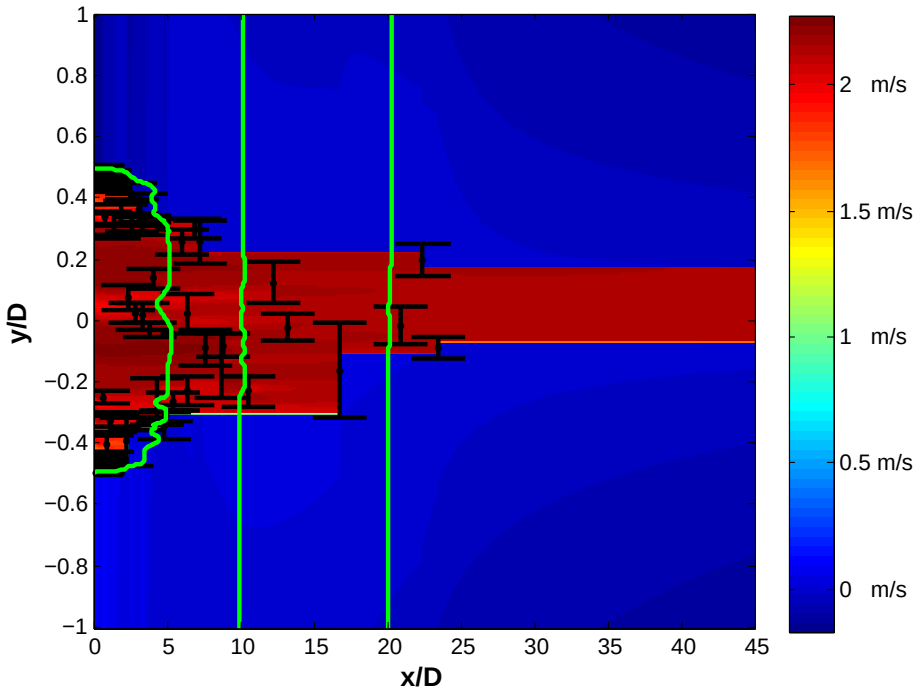

Figure 5: Jet velocity field and eddy occurrences for a simulated realization at Weber number 10^7. The liquid region is bounded above and below by black solid lines. Color in the liquid region indicates streamwise velocity in m/s. Green lines representing streamwise velocity profiles at $x/D = 0, 10$, and 20 show that the streamwise gas velocity is taken to be uniform and to match the liquid velocity at each phase interface. Color in the gas region indicates lateral velocity, whose spatial variation reflects the imposed linear z dependence, with slope on either side that increases linearly in time, and hence in x. The black bars indicate eddy sizes. and locations.

570 Fig. 5 shows the velocity field for a single simulated jet realization at a Weber number of 10^7 and the baseline values for the other variables that are shown in Table 2. In the figure, the streamwise location of the temporal evolving

solution on the ODT line is based on the liquid bulk velocity times the elapsed simulation time. The liquid phase region in Fig. 5 is separated from the gas phase by the black solid line. The black bars show the locations and the sizes of the accepted eddies. The absence of detached droplets in Fig. 5 reflect their removal upon detachment, as discussed earlier. The green lines are streamwise velocity profiles at $x/D = 0, 10$, and 20.

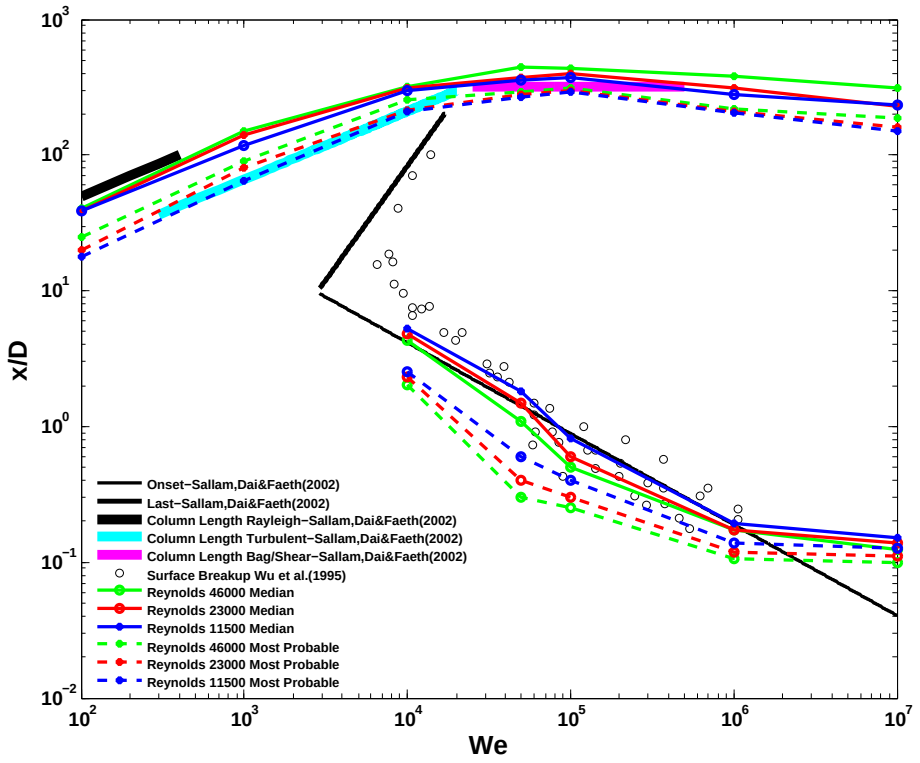

Figure 6: Breakup regime map.

Fig. 6 summarizes the main results of this study in a breakup regime map. The plotted model results correspond to the baseline conditions shown in Table 2 except for We and Re_{bulk}, which vary as indicated in the plot. The vertical axis shows the axial position x normalized by the jet diameter. Onset, and column length refer to the location of the onset of breakup, i.e. the axial position of the first multiphase eddy, and the length of the liquid core respectively. Wu and

Faeth (1995) and Sallam et al. (2002) suggested correlations for the onset and the length of the liquid core in terms of the liquid Weber number $We = \rho_l D u_0^2/\sigma$, where ρ_l is the liquid density, u_0 is the average liquid velocity at the jet exit, and σ is the surface tension of the liquid. Three modes of liquid-column breakup were identified by Sallam et al. (2002) for turbulent round liquid jets, as as described in section 2.7: a weakly turbulent Rayleigh-like breakup mode observed at low jet exit Weber number, a turbulent breakup mode observed at moderate jet exit Weber number, and an aerodynamic bag/shear breakup mode observed at high jet exit Weber number. The breakup-length correlation shown by Sallam et al. (2002) for each of these mechanisms is illustrated in Fig. 6. ODT results are shown for both the median and the most probable location based on an ensemble of 1000 realizations for each Weber and Reynolds number, indicated in Fig. 6 by solid and dashed lines, respectively. Since there is no clear indication that the correlations suggested by Sallam et al. (2002) are based on the mean, most probable, or other location statistic, both statistics are presented.

The Rayleigh term in the expression determining eddy likelihood is compatible in formulation with the theory of the Rayleigh and turbulent regimes of liquid-column breakup, and accordingly the ODT results match the slopes of the corresponding experimental correlations. As mentioned above, the heights of the experimental trend lines were matched by tuning the ODT Rayleigh parameter A. Likewise, the insensitivity of the liquid-column breakup length to Weber number in the bag/shear regime is reproduced by ODT and the height of the experimental trend line is matched by adjustment of the parameter S.

Fig. 7 shows the effect of the liquid/gas density ratio on the liquid-column breakup length of the jet. The range of studied density ratios is shown in Table 2. In addition to ODT results, theoretical studies by Gorokhovski (2001) and measurements by Lee and Spencer (1933) and Chehroudi et al. (1985) are shown. The Weber number of the liquid jet in the ODT simulations and the experimental value is $5 * 10^5$. The liquid jet Reynolds number is 23000. The vertical axis shows the jet breakup length normalized by the nozzle diameter and the horizontal axis shows the square root of the liquid/gas density ratio.

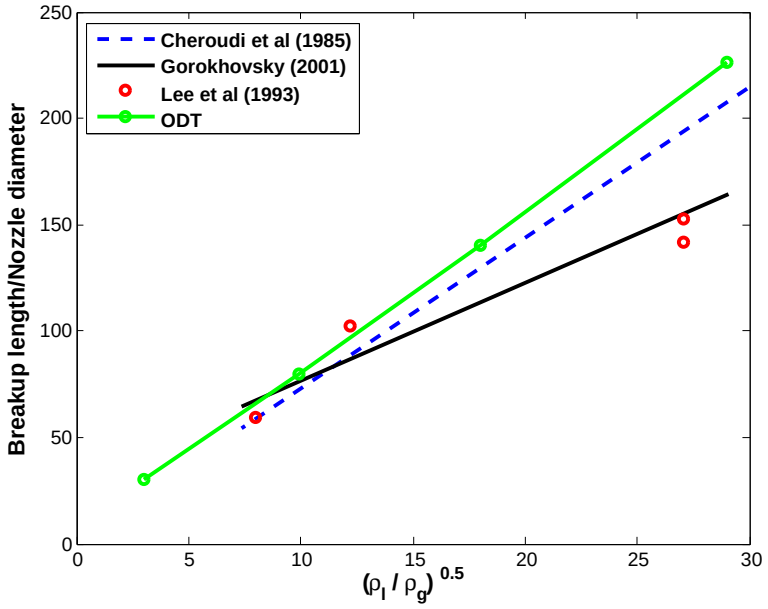

Figure 7: Breakup length as a function of the square root of the liquid/gas density ratio.

Although the absolute numbers exhibit considerable scatter, the results show that both ODT and the measurements obey the theoretical square-root dependence on the density ratio. The origin of this behavior in ODT is explained in section 2.9. The explanation is predicated on neglect of surface-tension effects (among other assumptions), explaining why the ODT representation of high-Weber-number jet breakup is insensitive to Weber number, a result that is supported by the Weber-number insensitivity of the jet breakup length seen in Fig. 6 at high Weber numbers.

The ODT numerical results indicate that the analysis in section 2.9, which assumes $\rho_l/\rho_g \gg 1$, is valid for values of this ratio at least as low as 10. This is not necessarily an indication that the square-root scaling is physically valid for such a low ratio, and presently there does not appear to be any clear evidence in this regard.

3.2.3. Onset and termination of droplet release

Turning from the topic of jet breakup length to the statistics of droplet

release from the intact liquid core, Fig. 6 indicates reasonable agreement of ODT results for the onset of droplet release with measurements. The degree of agreement depends on the statistical data reduction that is performed. The ODT simulations did not provide a discernible indication of the termination of droplet release, corresponding to the three highest data points of the plotted measurements by Wu et al. The lines labeled Onset and Last are based on their theoretical analysis of the onset and termination mechanisms. Termination refers to the last turbulent breakup occurring at the jet surface before the jet intact core fully breaks. The elaped-time criterion parameter β is tuned to the value 0.14 for best agreement with the onset of breakup measurements. ODT dynamics capture the measured trend with respect to Weber number irrespective of the precise choice of β.

Fig. 8 shows the dependence of the onset location on Re_{bulk} for Weber number fixed at 10^5 and other parameters assigned their baseline values, except that additional cases are shown for which $S = 0$ instead of its baseline value. The dependence is evaluated based on variation of Re_{bulk} by varying either u_{bulk} or the liquid viscosity. The Re_{bulk} value that falls outside the plot frame is 92000.

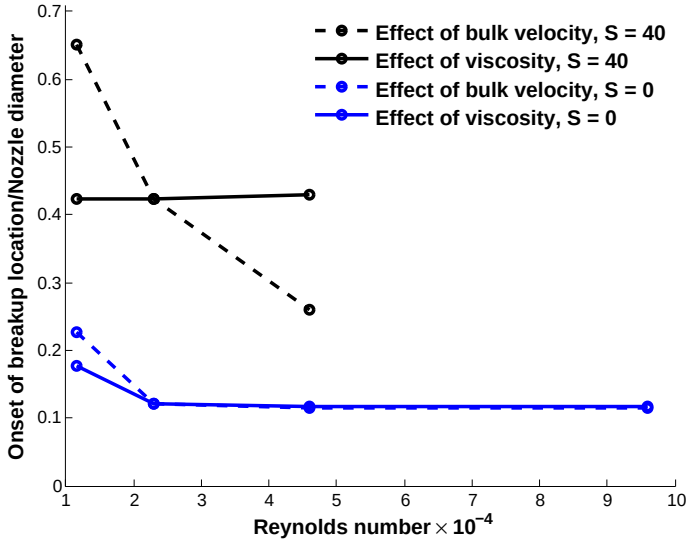

Figure 8: Re_{bulk} dependence of breakup onset location for $We = 10^5$.

For the baseline S value, the dependence is sensitive to the method of varying Re_{bulk}, indicating that some other parameter in addition to Re_{bulk} and We is needed to collapse the normalized properties of the breakup process. Reduction of the aerodynamic coupling by choosing $S = 0$ greatly reduces this sensitivity, indicating that aerodynamic coupling, which can introduce additional length and time scales and thus, e.g., an additional Reynolds number, is the cause of the sensitivity.

Faeth and coauthors do not discuss the Re_{bulk} dependence of breakup onset location but the measurements shown on their regime map and the information in their legends enable Re_{bulk} to be inferred for each measurement. The collection of cases was not configured to enable straightforward determination of the Re_{bulk} dependence for fixed We, but a detailed inference procedure allowed this determination. The specifics of the procedure and the various implications of the results are beyond the scope of the work presented here so they will be reported elsewhere. What is pertinent here is the conclusion that no statistically significant dependence on Re_{bulk} could be discerned but a mild dependence might exist below the threshold of statistical significance.

On this basis, the $S = 0$ results in Fig. 8 are consistent with the Re_{bulk} dependence implied by the measurements but the results for the baseline S value are not. Thus the baseline S value, though suitable for obtaining the correct jet length at high We, results in too much near-field aerodynamic shear. This indicates that the linear-in-time shear model, notwithstanding the beneficial feature that it introduces the correct dependence of jet length on the density ratio, is too simple for a correct near-field treatment and needs some elaboration in that regard. This will be addressed in future work.

Aerodynamic shear has two effects on jet breakup. The most important far-field effect is to augment breakup by promoting jet instability. In the near field, the model results imply that a more important effect is to promote the viscous transport of liquid momentum to the gas phase, with effects on the flow structure that delay the onset of breakup. This is indicated by the earlier onset of breakup when the aerodynamic effect is reduced. This not necessarily physically realistic

and further motivates future improvement of the shear treatment. Any such change is likely to require modification of the parameter β in order to maintain the ODT onset location versus We curve at the experimentally observed level.

3.2.4. Droplet statistics

ODT can generate a distribution of droplet sizes which, e.g., can serve as an input for subsequent secondary breakup models in CFD simulations. However, as ODT as presented here provides droplet sizes from primary breakup only, comparisons with experiments, which usually cannot separate droplets from primary and secondary breakup, should be regarded as tentative. Here we use a study by Sallam and Faeth (2003) for a qualitative comparison and scaling results.

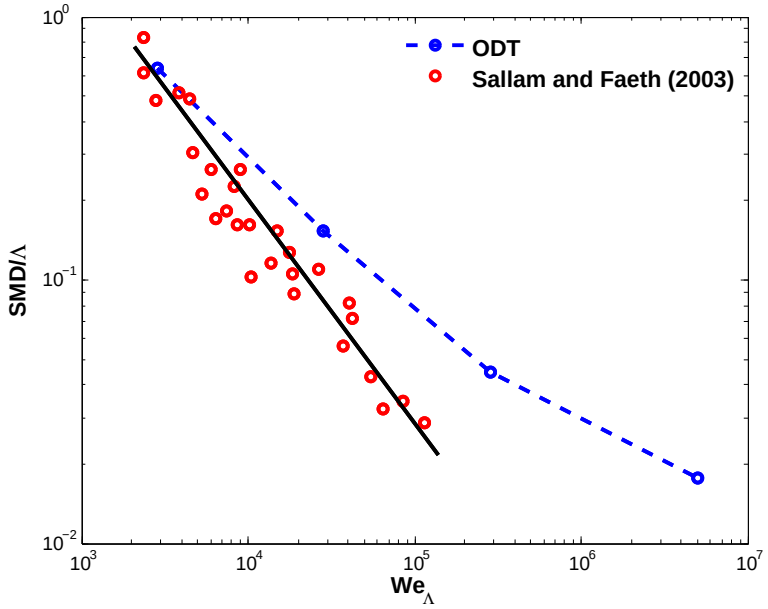

Figure 9: Droplet diameters at the onset of their formation along the surface of liquid jet as a function of the Weber number.

Fig. 9 shows droplet diameters at the onset of their formation along the surface of the jet at different Weber numbers. This study is based on the baseline values summarized in Table 2 except the Weber number values which

are in the range of $10^4 - 10^7$. The black solid line shows the best fit correlation of the measurements reported by Sallam and Faeth (2003). The vertical axis shows the droplet Sauter Mean Diameter (SMD) normalized by Λ, which is the cross stream integral length scale of the flow at the jet exit. Based on Sallam and Faeth (2003), Λ scales with the hydraulic diameter d_h which corresponds to the channel diameter here. The horizontal axis shows the jet exit Weber number based on Λ. Results show consistency versus experiments but with a lower rate of decrease as Weber number increases. This might be due to the above mentioned fact that ODT considers droplets resulting from primary breakup only whereas the experimental results will contain secondary breakup effects as well, leading to overall smaller droplets.

Physical modeling described in the Appendix is needed in order to infer physical droplet statistics from the statistics of ODT droplet-formation events. This modeling introduces a tunable parameter B in section Appendix .3 that relates ODT and physical droplet sizes. For the data comparison shown in Fig. 9, an equivalent tuning was performed by adjusting the value of Λ such that the ratio Λ/D is equal to 2/7.

Fig. 10 shows the variation of the Sauter Mean Diameter (SMD) of droplets released via primary breakup as a function of the distance from the nozzle for different Weber numbers. This study is based on the baseline values summarized in Table 2 except the Weber number values which are in the range of $10^4 - 10^6$. The vertical axis shows the SMD normalized by Λ and the horizontal axis shows the distance from the nozzle normalized by $\Lambda We_\Lambda^{1/2}$. The circular symbols show the measurements by Sallam and Faeth (2003) with the jet exit Weber number within the range 200 - 300,000. The square symbols represents the most probable location of column breakup for different Weber numbers. As results show ODT curves extend beyond column breakup location because that refers to the most probable location in 2000 realization and therefore breakup extends beyond that point for some realizations. The droplet statistics are collected cumulatively as has been described in Appendix .3. As the results show, the droplet size linearly increases with increasing distance from the nozzle.

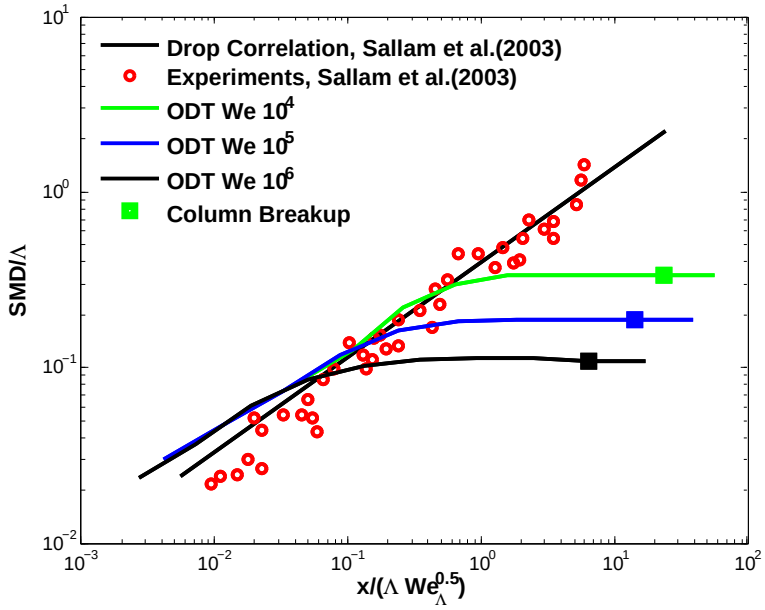

Figure 10: Droplet diameters along the surface of liquid jet function of Weber number and distance from the nozzle. The square symbols show the most probable location of column breakup at different Weber numbers.

This process continues until far downstream where aerodynamic shear breakup mechanism dominates. The model representation of this mechanism, which is formulated to reproduce the We and density-ratio dependence of column breakup length, fails to capture the measured upward continuation of the SMD trend far downstream in Fig. 10. This discrepancy is not surprising given the rudimentary treatment of aerodynamic shear effects in the model.

Advanced measurement techniques and numerical simulations are progressing toward achieving the capability to generate size distributions of primary-breakup droplets. This will allow detailed, unambiguous validation of the modeling approach presented here and thereby indicate its future prospects for becoming a robust predictive tool.

4. Conclusion

In this study, we propose a new model to predict primary breakup of liquid jets. The model is based on extensions to the stochastic One-Dimensional Turbulence model (ODT) that incorporate surface tension and its interaction with liquid-phase turbulence, Rayleigh waves and aerodynamic shear. Simulations are performed, starting with a liquid jet with no breakup to investigate turbulence levels inside a jet and followed by a jet with primary breakup. The simulations span the Weber number range $[10^2 - 10^7]$ at three different Reynolds numbers: 11500, 23000 and 46000. The liquid/gas density ratio ranges from 10 to 860.

The major conclusions of this study are as follows:

- After parameter adjustments, ODT reproduced column-breakup results reported previously by Wu and Faeth (1995) and Sallam et al. (2002) encompassing the weakly turbulent Rayleigh-like breakup, turbulent breakup, and aerodynamic bag/shear breakup regimes.
- ODT results for the most probable and the median location of onset of breakup show agreement with the experiments, including sensitivity to Weber number but not to Reynolds number. The latter result reflects an apparent deficiency of the aerodynamic shear treatment in the near field.
- Based on an assumed rate of streamwise increase of the strength of aerodynamic shear effects, ODT yields a square-root dependence of the jet column-breakup length on the liquid-to-gas density ratio in the shear-dominated (high Weber number) regime, as found experimentally and explained by previous analysis.
- The Sauter mean diameter of the droplets at the onset of their formation decreases with increasing Weber number. The ODT results show the same trend as experiments but with lower slope.

Some of the noted results reflect incorporation into ODT of empirical phenomenology that is largely based on dimensional reasoning. Extended in this

manner, ODT is capable of generating droplet formation statistics that are otherwise available only from costly multidimensional flow simulations. This enables model application over a broader parameter range than is affordable using other methods.

The proposed model has the potential to include further physical mechanisms influencing primary breakup, e.g. viscosity and surface-tension variability due to thermal non-uniformity, and effects of evaporation, including compositional non-uniformity due to fractional distillation of multi-component fuels. Extensions to cavitating and supercritical conditions are also envisioned.

5. Acknowledgments

The authors thank the Knut & Alice Wallenberg Foundation for financial support of this project.

Appendix: Interpretation of ODT droplet statistics

Appendix .1. Overview

In the ODT breakup model, the ODT domain nominally represents a lateral line of sight through the liquid jet. ODT is formulated to represent flows that are statistically homogeneous in directions normal to the ODT domain, so the physical configuration to which the ODT breakup model most directly applies is the planar jet. Nevertheless, it is possible to apply the breakup model to round jets in a physically and mathematically consistent way.

For some purposes, this is straightforward. The regime map in section 3.2 shows the Weber-number dependence of the streamwise location of the occurrence of particular stages of breakup (onset of breakup, final jet breakup). The determination of these locations in ODT breakup simulations is straightforward. However, determination of the physical quantities corresponding to ODT droplet statistics requires detailed consideration, as follows.

An ODT multiphase eddy breaks the liquid region into either two or three disconnected segments, where the latter case is interpreted as the occurrence of

final jet breakup. Final jet breakup does not contribute to the droplet statistics presented here, so only the case of breakup into two segments is considered. As illustrated in Fig. 2, this corresponds to a situation in which the eddy initially contains only one phase interface. The triplet map then creates three compressed copies of the liquid region that it contains, one of which remains attached to the liquid core while the other two, which are contiguous, form a newly separated liquid region that is deemed to be a released droplet.

Two aspects of model interpretation are addressed. One is the enforcement of conservation laws, in particular, mass conservation. The second is the interpretation of the ODT domain as a transverse line that is swept downstream at the liquid bulk velocity u_{bulk}, such that droplet releases can be detected only at the streamwise location $x = u_{bulk}t$ at any given time t.

To address the first point, a geometrical interpretation of ODT application to a round jet is invoked. The ODT breakup simulation is initialized with a liquid segment of lateral extent D corresponding to the jet diameter at the injector orifice. Accordingly, the lateral extent $D(x)$ of the ODT liquid core at any $x \geq 0$ is deemed to represent the jet diameter at x, where $D(0)$ corresponds to D with no argument. For all x, the jet cross-section is assumed to be circular. Assuming that the liquid bulk velocity u_{bulk} is constant in x, the jet streamwise mass flux at x is $\frac{\pi}{4}u_{bulk}\rho_l D^2(x)$. The decrease of $D(x)$ with x due to droplet releases implies reduction of the jet streamwise mass flux and a commensurate increase of the streamwise mass flux of the dispersed liquid (the released droplets).

This interpretation implicitly addresses the second point. Namely, advancement of an ODT realization in time t is interpreted for statistical purposes advancement along the streamwise coordinate $x = u_{bulk}t$. On this basis, each ODT realization is deemed to specify an x-dependent steady (time-invariant) jet streamwise mass flux. Then release of an ODT droplet corresponds to a reduction of the jet streamwise mass flux at the release location, implying a commensurate rate of conversion of jet mass into droplet mass. Based on a determination of droplet size that is explained in Appendix .3, the statistics of droplet releases during an ensemble of ODT realizations are used to determine

both the mean rate of statistically steady droplet creation as a function of x and the droplet size distribution.

Appendix .2. Liquid core mass-loss rate

The most fundamental breakup statistic is the rate of breakup-induced mass loss from the jet. To show how this is inferred from ODT output, the jet mass-loss rate is first evaluated for a single ODT droplet release at some location $\hat{x}$. That release abruptly reduces $D(x)$ from $D_-(\hat{x})$ to $D_+(\hat{x})$, where the subscripts $-$ and $+$ denote values upstream and downstream of the discontinuity, respectively. Based on the constant liquid bulk velocity u_{bulk}, the associated change of jet streamwise mass flux at $\hat{x}$ is $\phi = \frac{\pi}{4} u_{bulk} \rho_l [{D_+}^2(\hat{x}) - {D_-}^2(\hat{x})]$. $-\phi$, which is positive, is interpreted as the associated increase of the streamwise droplet mass flux. Henceforth, the minus sign is dropped and ϕ is taken to be the absolute value of the indicated expression.

This result assumes that the ODT release event represents a steady process of jet-to-droplet mass-flux conversion at $\hat{x}$, or more generally, at the locations x_i of the droplet releases during one ODT realization. As in experiments, the quantity of interest is the time-averaged rate of streamwise mass-flux transfer from the jet to the droplets as a function of x.

As explained in Appendix .1, each ODT realization generates, in effect, a representation of droplet releases along the space-time trajectory $x = u_{bulk} t$. Any epoch t corresponds to one location $x(t)$ along this trajectory. Therefore ODT cannot directly provide time-averaged information as a function of x. However, an ensemble of ODT realizations can provide ensemble statistics as a function of x, which constitute an equivalent representation of droplet statistics gathered during measurements of statistically steady jet breakup, assuming ergodicity of both the model and the corresponding physical process.

On this basis, the x dependence of the mean rate of core-to-droplet mass conversion is determined from ODT output as follows. The fundamental quantity of interest the cumulative jet-to-droplet mass-flux conversion $\Phi(x)$ within the streamwise interval $[0, x]$. For one ODT realization, this can be expressed

as $\Phi(x) = \sum_{i=1}^{I(x)} \phi_i$, where $\phi_i = \frac{\pi}{4} u_{bulk} \rho_l |{D_+}^2(x_i) - {D_-}^2(x_i)|$ is the jet-to-dispersed-phase streamwise mass-flux conversion associated with the ith droplet release and $I(x)$ is the largest value of i for which the location x_i of the release does not exceed x. Φ is piecewise constant in x with a discontinuity wherever $x = x_i$ for some i.

Each member j of a collection of J ODT realizations yields the output $\Phi_j(x)$ for the realization. Averaging over j gives an estimate $\langle \Phi(x) \rangle_J$ of the desired ensemble average $\langle \Phi(x) \rangle$. For any finite J, $\langle \Phi(x) \rangle_J$ is piecewise constant, but for large J, this estimate converges to the ensemble ($J = \infty$) limit, which is a continuous function of x. A differentiable approximant of $\langle \Phi(x) \rangle$ can be obtained by filtering or by fitting a smooth function to $\langle \Phi(x) \rangle_J$.

This enables estimation of the ensemble average rate of jet-to-dispersed-phase streamwise mass-flux conversion per unit streamwise distance $\langle \phi \rangle = \frac{d}{dx} \langle \Phi \rangle$. $\langle \phi \rangle$ could be estimated directly in terms of the collection of quantities ϕ for J realization, but evaluating it using $\langle \Phi \rangle$ is convenient because it circumvents the handling of discontinuities, as in the estimation of a probability density function from data by differentiating a smoothed estimate of the cumulative distribution.

$\langle \Phi(x) \rangle$ can be interpreted as the droplet mass flux at x only if the streamwise velocity of all droplets at all x is u_{bulk}, which is generally incorrect owing to liquid-gas momentum and mass exchange and other effects. Therefore model results evaluate only the contribution $\langle \phi(x) \rangle$ of newly released droplets to the droplet mass flux. Further modeling beyond the present scope is needed to evaluate droplet evolution after release.

Appendix .3. Droplet size distribution

$\langle \phi(x) \rangle$ can be used to determine the mean rate $r(x)$ of droplet releases per unit streamwise distance based on droplet size information. For example, if the droplets are monodisperse with mass m, then $r(x) = m^{-1} \langle \phi(x) \rangle$, where $m(s) = \frac{\pi}{6} \rho_l s^3$ for droplet diameter s.

Upon release, a given ODT droplet occupies some length-l_d interval of the ODT domain. As explained shortly, l_d is used to identify an associated physical

droplet diameter s and mass $m(s)$. s is assumed to be the diameter of each of the physical droplets comprising the steady mass flux attributed to the ODT droplet release event.

Each of these events yields a different ODT droplet size l_d and therefore a different physical diameter s. The collection of events during an ensemble of ODT realizations thus generates a polydispersion. To gather the associated droplet-size statistics, the range of droplet diameters s is discretized into bins $k = 1, \ldots, K$, where each bin is assigned a nominal diameter s_k and mass m_k.

The events that produce droplets within the diameter range of bin k constitute a size-conditioned subset of all droplet release events. Accordingly, the formal development in Appendix .2 is applied on a size-conditioned basis. Namely, $\Phi_k(x)$ is the jet mass-flux loss attributed to events that release droplets in the bin-k diameter range. $\langle \phi_k \rangle$ is obtained from $\langle \Phi_k \rangle$ in the same manner as $\langle \phi \rangle$ is obtained from $\langle \Phi \rangle$. This enables the determination of the bin quantities $\langle r_k(x) \rangle = m_k^{-1} \langle \phi_k(x) \rangle$. By dividing each quantity $\langle r_k(x) \rangle$ by $\sum_{k=1}^{K} \langle r_k(x) \rangle$, the normalized histogram (discrete form of the probability density function) of droplet diameter is obtained. Specifically, this determines the size distribution of droplets released at the streamwise location x.

The remaining consideration is to associate a diameter s with a given droplet release in ODT. The available physical input is the size l_d of the liquid interval representing the droplet. This is a physically relevant length scale because it reflects the scale of the physical mechanisms of droplet separation from the liquid core as they are represented in ODT (see section 2). However, the modeling of these mechanisms does not capture behavior in directions not aligned with the ODT domain such as the distortion of the shape of the phase interface as the droplet is formed. Therefore the size of the droplet in ODT is at best a rough estimate of the physical droplet diameter. Accordingly, the droplet diameter s is expressed as $s = B l_d$, where B is a tunable coefficient. Because B is a single number that can hopefully be assigned a case-independent value while the droplet generation rate is a function of streamwise location, Weber number, ρ_l/ρ_g, and other quantities, there is ample scope to fit B to a subset of the

available data and subsequently validate the various parameter dependences predicted by the model.

Appendix .4. Discussion

As noted in Appendix .1, ODT has a consistent physical interpretation as a representation of flows that are statistically homogeneous in directions normal to the ODT domain. The application of ODT to a round jet is not fully consistent by construction, but it approaches physical consistency in a particular limit, as described next.

The physically consistent limit of the round-jet application described here is the regime $l_d \ll D$. The ODT droplet scale l_d is the scale of the physical mechanisms of droplet generation. At scales much less than D, the mean shape of the perimeter of the liquid core is planar to a good approximation, so modeling of processes that generate small droplets using a planar-jet picture is a reasonable idealization. Those processes are of course coupled to the core flow and therefore are in principle geometry dependent, but this introduces at most an order-one error that is subsumed into parameter adjustments.

These considerations justify the physical interpretation of ODT primary-droplet generation from a dimensional scaling viewpoint, but they do not account for the intermediate step of ligament formation, followed by ligament breakup into droplets. A possible empirical representation of this process would be to treat ODT droplet release as physical droplet release farther downstream, reflecting the time required for ligament breakup. Ligament lifetime determination as in Sallam and Faeth (2003) could be the basis for such a representation.

References

Apte SV, Gorokhokhovski M, Moin P. LES of atomizing spray with stochastic modeling of secondary breakup. International Journal of Multiphase Flow 2003;29:1503–22.

Apte SV, Mahesh K, Gorokhokhovski M, Moin P. Stochastic modeling of atomizing spray in a complex swirl injector using large eddy simulation. Proceedings of the Combustion Institute 2009;32:2257–66.

Ashurst WT, Kerstein AR. One-dimensional turbulence: Variable-density formulation and application to mixing layers. Physics of Fluids 2005;17:025107.

Ashurst WT, Kerstein AR. Erratum to One-dimensional turbulence: Variable-density formulation and application to mixing layers. Physics of Fluids 2009;21:119901.

Chehroudi B, Chen SH, Bracco FV, Onuma Y. On the intact core of full-cone sprays. SAE Technical Paper 1985;850126.

Chesnel J, Ménard T, Réveillon J, Demoulin FX. Subgrid analysis of liquid jet atomization. Atomization and Sprays 2011;21:41–67.

Chiu SN, Stoyan D, Kendall WS, Mecke J. Stochastic geometry and its applications. John Wiley & Sons, 2013.

Dam NV, Rutland C. Adapting diesel large-eddy simulation spray models for direct-injection spark-ignition applications. International Journal of Engine Research 2015;in press.

Desjardins O, Moureau V, Pitsch H. An accurate conservative level set/ghost fluid method for simulating turbulent atomization. Journal of Computational Physics 2008;227:8395–8416.

Echekki T, Kerstein AR, Chen JY, Dreeben TD. One-dimensional turbulence simulation of turbulent jet diffusion flames: Model formulation and illustrative applications. Combustion and Flame 2001;125:1083–1105.

Gonzalez-Juez ED, Schmidt RC, Kerstein AR. ODTLES simulations of wall-bounded flows. Physics of Fluids 2011;23:125102.

Gorokhovski M. The stochastic Lagrangian model of drop breakup in the computation of liquid sprays. Atomization and Sprays 2001;11:1514–24.

Herrmann M. Detailed numerical simulations of the primary atomization of a turbulent liquid jet in crossflow. Journal of Engineering for Gas Turbines and Power 2010;132:061506.

Herrmann M. The influence of density ratio on the primary atomization of turbulent liquid jet in crossflow. Proceedings of the Combustion Institute 2011;33:2079–88.

Hussain A, Reynolds W. Measurements in fully developed turbulent channel flow. Journal of Fluids Engineering 1975;97:568–578.

Jhavar R, Rutland CJ. Using large eddy simulations to study mixing effects in early injection diesel engine combustion. SAE Technical Paper 2006;2006-01-0871.

Kerstein A, Wunsch S. Simulation of a stably stratified atmospheric boundary layer using one-dimensional turbulence. Boundary Layer Meteorology 2006;118:325–356.

Kerstein AR. One-dimensional turbulence: Model formulation and application to homogeneous turbulence, shear flows, and buoyant stratified flows. Journal of Fluid Mechanics 1999;392:277–334.

Kerstein AR, Ashurst WT, Wunsch S, Nilsen V. One-dimensional turbulence: Vector formulation and application to free shear flow. Journal of Fluid Mechanics 2001;447:85–109.

Lebas R, Blokkeel G, Beau PA, Demoulin FX. Coupling vaporization model with the Eulerian-Lagrangian spray atomization (ELSA) model in diesel engine conditions. SAE Technical Paper 2005;2005-01-0213.

Lebas R, Menard T, Beau P, Berlemont A, Demoulin FX. Numerical simulation of primary break-up and atomization: DNS and modelling study. International Journal of Multiphase Flow 2009;35:247–260.

Lee DW, Spencer RC. Photomicrographic studies of fuel sprays. volume 454. NACA, 1933.

Lignell D, Kerstein A, Sun G, Monson E. Mesh adaption for efficient multiscale implementation of one-dimensional turbulence. Theoretical and Computational Fluid Dynamics 2013;27:273–295.

Linne M. Imaging in the optically dense regions of a spray: A review of developing techniques. Progress in Energy and Combustion Science 2013;39:403–440.

Linne MA, Paciaroni M, Berrocal E, Sedarsky D. Ballistic imaging of liquid breakup processes in dense sprays. Proceedings of the Combustion Institute 2009;32:2147–61.

Mahesh K, Constantinescu G, Apte S, Iaccarino G, Ham F, Moin P. Large-eddy simulation of reacting turbulent flows in complex geometries. Journal of Applied Mechanics 2006;73:374–381.

Meiselbach FT. Application of ODT to turbulent flow problems. Ph.D. thesis; Brandenburg University of Technology; Cottbus, Germany; 2015.

Moser RD, Kim J, Mansour NN. Direct numerical simulation of turbulent channel flow up to Re=590. Physics of Fluids 1999;11:943–5.

Ning W, Reitz RD, Lippert AM, Diwakar R. Development of a next-generation spray and atomization model using an Eulerian-Lagrangian methodology. In: 17^{th} International Multidimensional Engine Modeling User's Group Meeting. Detroit, MI; 2007. .

O'Rourke PJ, Amsden AA. The TAB method for numerical calculation of spray droplet breakup. SAE Technical Paper 1987;872089.

Reitz RD. Modeling atomization processes in high-pressure vaporizing sprays. Atomisation and Spray Technology 1987;3:309–37.

Ross SM. Stochastic Processes. 2nd ed. John Wiley & Sons New York, 1996.

Sallam K, Dai Z, Faeth G. Liquid breakup at the surface of turbulent round liquid jets in still gases. International Journal of Multiphase Flow 2002;28:427–49.

Sallam K, Faeth G. Surface properties during primary breakup of turbulent liquid jets in still air. AIAA Journal 2003;41:1514–24.

Schmidt RC, Kerstein AR, Wunsch S, Nilsen V. Near-wall LES closure based on one-dimensional turbulence modeling. Journal of Computational Physics 2003;186:317–55.

Schulz FT, Glawe C, Schmidt H, Kerstein AR. Toward modeling of CO2 multiphase flow patterns using a stochastic multi-scale approach. Environmental Earth Eciences 2013;70:3739–48.

Shinjo J, Umemura A. Simulation of liquid jet primary breakup: Dynamics of ligament and droplet formation. International Journal of Multiphase Flow 2010;36:513–32.

Shinjo J, Umemura A. Detailed simulation of primary atomization mechanism in Diesel jet sprays (isolated identification of liquid jet tip effects). Proceedings of the Combustion Institute 2011;33:2089–97.

Tanner F. Liquid jet atomization and droplet breakup modeling of non-evaporating diesel fuel sprays. SAE Technical Paper 1997;970050.

Toninin S, Gavaises M, Theodorakakos A. Modelling high-pressure dense diesel sprays with adaptive local grid refinement. International Journal of Heat and Fluid Flow 2008;29:427–48.

Vallet A, Burluka AA, Borghi R. Development of an Eulerian model for atomization of a liquid jet. Atomization and Sprays 2001;11:619–642.

Wolf D, Incropera F, Viskanta R. Measurement of the turbulent flow field in a free-surface jet of water. Experiments in Fluids 1995;18:397–408.

Wu PK, Faeth G. Aerodynamic effects on primary breakup of turbulent liquids. Atomization and Sprays 1993;3:265–289.

Wu PK, Faeth G. Onset and end of drop formation along the surface of turbulent liquid jets in still gases. Physics of Fluids 1995;7:2915–7.